Available online at www.sciencedirect.com

ScienceDirect

Procedia CIRP 124 (2024) 20–23

www.elsevier.com/locate/procedia

13th CIRP Conference on Photonic Technologies [LANE 2024], 15-19 September 2024, Fürth, Germany

# The effect of in-source spatial beam shaping on the laser welding of e-mobility metals and alloys

Francesco Galbusera[a]*, Giulio Borzoni[a], Simone D'Arcangelo[a], Leonardo Caprio[a], Barbara Previtali[a], Ali Gökhan Demir[a]

[a]*Department of Mechanical Engineering, Politecnico di Milano, Via La Masa 1, I-20156 Milan, Italy*

* Corresponding author. Tel.: +39 3345734189. *E-mail address:* francesco.galbusera@polimi.it

**Abstract**

Electromobility applications require several welded connections using demanding materials often in dissimilar combinations. Copper, aluminium, or steel alloys are laser welded for energy storage and traction related components. On the one hand, high power fiber laser sources provide in-source beam shaping solutions able to modify the irradiance profile towards ring-shaped beams. On the other hand, research focused on the effect of the beam shapes on the melting mechanisms and process quality is still in progress. This work studies the effect of different beam profiles on AISI301LN, AA6082 and pure Cu with a 5 kW fiber laser. Linear trends of power over penetration depth as a function of speed confirms the validity of employing the lumped heat capacity model for ring-shaped beams. Moreover, the specific melting fluence is observed to exhibit an exponential decaying trend with the proportion of power allocated in the fiber core, irrespective of tested material.



*Keywords:* Beam shaping; Laser welding; Battery pack; Electric drive

## 1. Introduction

Electrification is transforming mobility by promoting electric powertrains and related power storage units. The demanding quality standards involved into the battery packs, e-motors and power electronics of next generation vehicle necessitate robust manufacturing solutions [1]. This pertains to joints composed of dissimilar materials, such as Al-Cu/Steel-Al, containing brittle intermetallics [2–4], or the welding of hairpin made of copper, whose high-reflectivity to industrial fiber laser results into melting instabilities and porosities [5]. Laser welding emerges as an effective solution, and beam shaping can significantly enhance process flexibility. With the advent of industrial sources capable of manipulating the Power Density Distribution (PDD) of the beam, the laser tool can be flexibly tailored to suit specific application. With such solutions, ring-shaped beams, combining Gaussian and toroidal intensities [6], have aided in stabilizing the welding process. This has resulted in the reduction of pores, spatter [7,8] or intermetallic formation in joints made of dissimilar materials [9], while providing greater control over the weld geometry. There is an evident need for parametric studies concerning to better understand the separate influence of core and ring contributions to the weld geometry and melting efficiency.

This study investigates the application of a dynamic in-source beam shaping solution to three e-mobility materials (AISI301LN, AA6082, and pure Cu) through bead-on-plate tests. Efficiency, measured in terms of penetration depth for different materials and PDDs, is benchmarked by estimating the required fluence using the lumped heat capacity model.

## 2. Materials and methods

### *2.1. Laser source and optical architecture*

A multi-core fiber laser with in-source beam shaping capabilities was utilized (Corona nLIGHT CFX 5000, nLIGHT, Vancouver, USA). This source features a double-ring structure of the fiber surrounding the central core. Capable of

2212-8271 
10.1016/j.procir.2024.08.063

emitting at a maximum power of 5 kW, the system allows for programming the power partition within its concentric structure, enabling operation with fourteen PDDs . Depending on the power allocation in the multi-core structure, the beam shape varies from Gaussian to doughnut-like distributions. To identify the profile, the nomenclature $P_c/P_{r1}/P_{r2}$ was used, where $P_c$, $P_{r1}$ and $P_{r2}$ indicate the proportion of power allocated in the core, first ring and second ring, respectively, declared by the laser manufacturer.

The optical architecture consisted of a scanner (Optoprim, Vimercate, Italy) designed for high-power fiber lasers. The head incorporated a set of lenses for collimating, conveying, manipulating and focusing the laser beam emitted from source.

### *2.2. Experimental procedures and analysis*

Three reference materials were selected for the investigation: AISI301LN stainless steel, AA6082 high-strength aluminum alloy and pure copper. Bead-on-plate tests were executed using a fixed laser power of 5 kW, an optical magnification of 3.125 and the focal plane of the PDD set on the top surface of the substrates. Scan speed and $P_c/P_{r1}/P_{r2}$ were varied based on the material being tested. Linear welds of 50 mm were realized on substrates with thickness higher than 5 mm and made of the reference materials. Table 1 summarizes the fixed and varied parameters tested.

Table 1. Fixed and varied process parameters.

| **Fixed parameters** | | |
|---|---|---|
| Laser power P (W) | Optical magnification M (-) | Focus position f (mm) |
| 5000 | 3.125 | 0 |
| **Varied parameters** | | |
| Material | Scan speed v (mm/s) | Power partition $P_c/P_{r1}/P_{r2}$ (%) |
| AISI301LN | 250 – 750 (step 250) | All |
| AA6082 | 100 – 500 (step 100) | 04-92/03-91/04-16 |
| Cu | 100 – 300 (step 100) | 30-92/03-54/04-17 |

The PDDs were characterized at the focal plane using a fixed power of 1 kW with a FocusMonitor FM+ (PRIMES GmbH, Pfungstadt, Germany). Some of the tested beam profiles are illustrated in Fig. 1, presenting relative intensity ($I/I_0$) normalized to the peak of the closest Gaussian distribution available (92/03/04 power ratio) and radial coordinate ($r$). As depicted, redistributing the same laser power across the multi-core structure of the fiber resulted in a decrease of the intensity peak at the center of the PDD and an increase in the spot size. Moreover, Fig. 1 illustrates that below a $P_c$ of 50%, the profiles exhibited a ring intensity located at radius of approximately 150 µm, deviating from a Gaussian-like distribution.

The linear welds were sectioned in different points and examined with conventional metallographic procedures. For each experimental condition, the weld geometry was measured in terms of penetration depth, $h$, and the ratio power over penetration depth, $P/h$, was calculated. This ratio defines a penetration efficiency that depends on the speed and the PDD. According to the lumped heat capacity model of Eqn. 1 [10]:

$$\frac{P}{h} = \frac{wv\rho}{A}\left(c_p\left(T_f - T_0\right) + L_f + m'L_v\right) \quad (1)$$

where $P$ is the power, $h$ the penetration depth, $w$ the weld width, $\rho$ the density, $A$ the optical absorptivity, $c_p$ the specific heat, $T_f$ the melting temperature, $T_0$ the ambient temperature, $L_f$ the enthalpy of fusion, $m'$ the fraction of vaporized material and $L_v$ the enthalpy of vaporization.

For a specific material, gas, optical architecture, and melting mechanism type (keyhole or conduction) it can be empirically demonstrated that $P/h$ exhibits a consistently increasing linear trend with scan speed:

$$\frac{P}{h} = F\,v \quad (2)$$

where $F$, the slope, represents the required specific fluence needed to melt the material and vaporize it if $m'$ is not negligible. For a Gaussian beam, this formulation can predict the melting mechanism and the penetration depth for a given material. However, for non-Gaussian beams, the linearity of the $P/h$ ratio may not necessarily hold true.

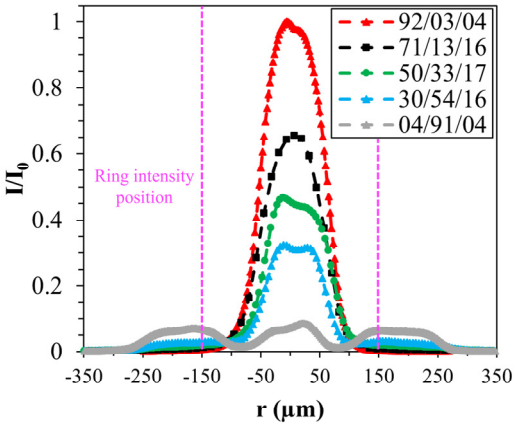


Fig. 1. Irradiance profiles expressed in terms of $I/I_0$ at $P$ = 1000 W where $I_0$ corresponds to 8.28 MW/cm$^2$. Purple dashed lines define the position of the ring intensity for the profiles 30/54/16 and 04/91/04.

This study evaluates the application of the model described in Eqn. 2 to different e-mobility materials and PDDs. The dataset utilizes penetration depth measurements for the computation of $P/h$ and $F$. The occurrence of defects, such as keyhole porosity in all the materials or hot cracks in AA6082, which may be related to an unoptimized set of process parameters, is therefore disregarded for the scope of this work.

## 3. Results

From the linear welds, it was observed that the penetration depth $h$ decreased with scan speed $v$ regardless of the PDD and the material. Moreover, at the same $v$ level and irrespective of the material, $h$ decreased when reducing the core power percentage $P_c$. Fig. 2 depicts some representative metallographic cross sections obtained with the processed materials for two power ratios, 92/03/04 and 30/54/16, and similar scan speed levels.

Fig. 3 shows power over penetration depth ratio $P/h$ as a function of speed, for the tested PDDs and materials. Linear growing trends with $v$ were observed across all the PDD suggesting the applicability of the lumped heat model for ring beams. Additionally, by redistributing the power within the multi-core structure of the fiber, the slope of the linear trends increases regardless of the material.

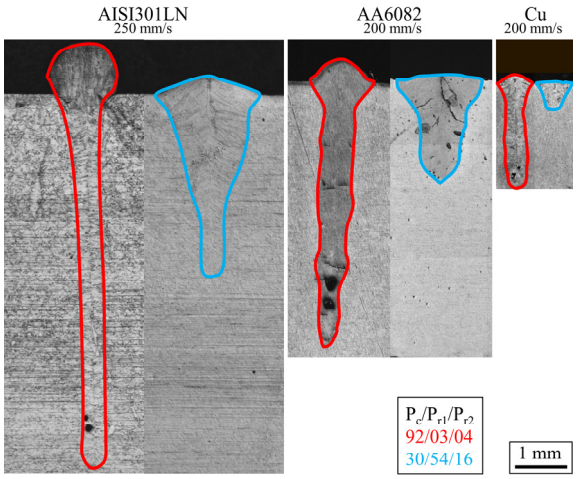


Fig. 2. Comparison of weld seams obtained for all the tested materials, two representative PDDs, 92/03/04 and 30/54/16, for similar processing speeds.

According to Eqn. 2, the slope of the *P/h* trends defines the specific fluence *F* required to melt, and vaporize if *m'* is not negligible, the material, at a given speed. This effect is linked with the reduction of intensity peak in the center of the PDDs, which is expected to influence the penetration depth for a given speed [11].

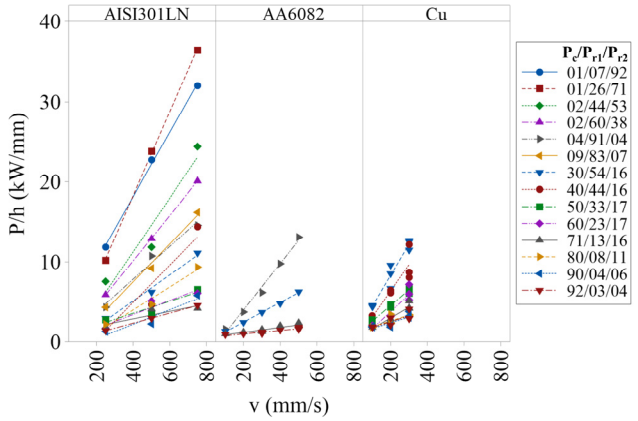


Fig. 3. Power to penetration depth ratio *P/h* (kW/mm) vs scan speed *v* (mm/s) for the tested materials. The nominal power allocation is used as a categorical filter. Colored lines denote the trends obtained with linear regression.

To visualize the effect of the beam profile on the specific melting fluence, estimates of *F* were derived through linear regression of the dataset. Consequently, the *F* data are depicted as a function of the core power percentage $P_c$ for each tested material in Fig. 4. Given that the laser power was fixed at 5 kW, each datapoint in this graph corresponds to a specific PDD. As shown, the specific fluence followed an exponential decaying trend with $P_c$, regardless of the material. For the AISI301LN and the AA6082 the gradual decrease defined a plateau region above 50 % and 70 % of $P_c$, respectively, where *F* exhibited minimal variation (less than 10 %) compared to the closest Gaussian beam, namely the 92/03/04 ratio. Conversely, for Cu the plateau was limited above 80 % of $P_c$, while below this threshold the curve exhibited rapid exponential growth. Welding was not feasible below a $P_c$ of 5 % for AA6082 and 30 % for Cu due to insufficient penetration. For AISI301LN, penetration was achieved using all the beam profiles, although below 2 % the required *F* was four times higher than that of a 92/03/04 profile (Gaussian-like profile).

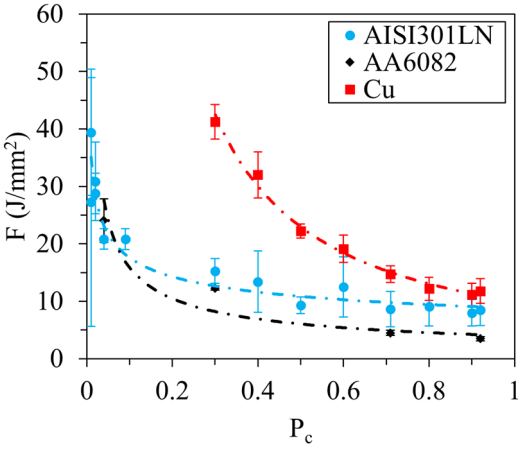


Fig. 4. Specific fluence *F* (J/mm²) vs core power percentage $P_c$ for each tested material. Dashed lines represent the fitting trends derived from nonlinear regression while error bars denote 95%CI for the mean.

The fitting of these datapoints enabled the definition of a set of parameters that could evaluate welding efficiency in terms of penetration depth for the tested materials and PDDs. Using the exponential trend presented in Eqn. 3:

$$F = \gamma \cdot P_c^{\beta} \quad (3)$$

where $\gamma$ and $\beta$ define the asymptote to a pure Gaussian condition, where all the power is ideally allocated in the core, and the curve growth rate, respectively. Table 2 shows the estimates and their corresponding 95 % confidence intervals fitted via nonlinear regression for each tested material.

Table 2. Nonlinear regression estimates and 95% Confidence Intervals (CI) for each tested material.

| Material | γ (95% CI) | β (95% CI) |
|---|---|---|
| AISI301LN | 9.32 (7.22; 11.5) | -0.28 (-0.35; -0.22) |
| AA6082 | 5.02 (1.99; 8.55) | -0.49 (-0.79; -0.28) |
| Cu | 10.1 (9.06; 11.3) | -1.18 (-1.30; -1.07) |

Notably, Cu presented the greatest challenge, as indicated by its higher $\gamma$ estimation, attributed to its high reflectivity to the near infrared wavelengths of the emitting source. Following Cu are AISI301LN and AA6082. Interestingly, despite aluminium's higher reflectivity compared to stainless steel, AA6082 showed a lower $\gamma$ estimate. This discrepancy likely arises from the value of *F* which depends on the product $c_p \Delta T_f$, favouring AISI301LN due to its higher melting temperature. However, the curve growth rate $\beta$ of AA6082, in absolute terms, is higher than $\beta$ of steel suggesting that below a certain threshold of $P_c$, melting of AISI301LN becomes easier than AA6082. Meanwhile, the growth rate $\beta$ of Cu surpasses, in absolute terms, those of AISI301LN and AA6082, indicating its greater demand for highly concentrated power density distributions, especially concerning penetration depth.

## 4. Discussion

This work studies the applicability of the lumped heat capacity model to various material, PDD and scan speed combinations, despite strong assumptions such as the temperature dependency of thermophysical properties or the beam waist equality with the weld width.

All the materials exhibited a specific fluence plateau, weakly dependent on power allocation in the fiber core, despite their different processability under the same wavelength. This effect demonstrates the importance of the intensity peak of each beam shape in determining the penetration depth. In this regard, ring-shaped beams obtained with a power redistribution mechanism are less efficient than Gaussian beams, when only penetration depth is considered. This point has to be considered in order to determine the power level choice of the laser source and make use of the additional benefits of the ring beams when addressing other challenges, such as the keyhole channel stability, the reduction of spatter and intermetallic formation in dissimilar joints [9,13]. These aspects become crucial in industrial applications for the e-mobility sector. A decaying trend of fluence following a power function with the increase of the core power was established empirically. With the same total power, the reduction in the core power results in a relatively wider beam. The cross-section images indicate a wider and a shallower bead when power is distributed along the core. It can be inferred that a wider and shallower capillary is formed throughout the welding operation when ring/core configurations are used. With a wider melt pool and a shallower keyhole, it can be hypothesized that more energy is lost to conduction and less energy of the laser beam is entrapped within the keyhole. Further modelling efforts are required to establish an analytical link between the beam power distribution and the processed depth similar to what has been established in Gaussian beams [12].

With industrial sources capable of shaping the beam and modern scanners offering flexibility in magnification, focusing, and oscillation, countless irradiance-based strategies can be explored. Therefore, to establish spatial beam shaping as a reproducible tool, it is essential to tune the beam properties for the application. This requires analytical modeling of the beam to develop generalized shape-encoding parameters that consider the actual structure of the PDD. Ultimately, integrating a bespoke PDD in simulative approaches can significantly aid in tailoring beam properties for specific applications, thus reducing experimental testing time.

## 5. Conclusions

In this study three representative e-mobility materials, AISI301LN, AA6082 and pure Cu, were processed with different speeds and ring-shaped beam profiles generated with a dynamic in-source beam shaping mechanism. A dataset of welding penetration depth was derived and interpreted with the lumped heat capacity model. The main results can be summarized as follows:

- All the materials featured a linear trend of power over penetration depth, *P/h*, as a function of speed and PDD, confirming the applicability of the lumped heat capacity model to non-Gaussian beams.
- The slope of the *P/h* trends, consisting of a specific melting fluence, followed an exponential decaying trend with the power percentage allocated in the fiber core $P_c$, regardless of the material.
- The materials featured a plateau region of specific fluence above a certain $P_c$ suggesting that irradiance can be tuned to produce similar penetration depth of a Gaussian beam while benefitting from the additional power in the fiber rings.

## Acknowledgements

The authors acknowledge the Italian Ministry of University and Education (MIUR) through the National Plan of Recovery and Resilience (PNRR). The authors are thankful to nLIGHT and Optoprim for the laser source and scanner used in the experimental activity. Laser Optronic and Primes are acknowledged for the support with the beam characterization.

## References

[1] M. Möller, P. Haug, P. Scheible, C. Buse, C. Frischkorn, N. Speker, Spatially tailored laser energy distribution using innovative optics for gas-tight welding of casted and wrought aluminum alloys in e-mobility, J Laser Appl 34 (2022) 042015. https://doi.org/10.2351/7.0000735.

[2] D. Wallerstein, F. Lusquiños, R. Comesaña, J. del Val, A. Riveiro, A. Badaoui, J. Pou, Dissimilar unbeveled butt joints of AA6061 to S235 structural steel by means of standard single beam fiber laser welding-brazing, J Mater Process Technol 291 (2021). https://doi.org/10.1016/j.jmatprotec.2020.116994.

[3] J. Coroado, S. Ganguly, S. Williams, W. Suder, S. Meco, G. Pardal, Comparison of continuous and pulsed wave lasers in keyhole welding of stainless-steel to aluminium, International Journal of Advanced Manufacturing Technology 119 (2022) 367–387. https://doi.org/10.1007/s00170-021-08226-5.

[4] A. Ascari, E.P. Zapico, V. Dimatteo, A. Fortunato, Dissimilar laser welding of copper and stainless-steel thin sheets for e-mobility applications, in: Procedia CIRP, Elsevier B.V., 2022: pp. 770–773. https://doi.org/10.1016/j.procir.2022.08.125.

[5] S. D'Arcangelo, L. Caprio, D. Chesi, D. Nocciolini, R. Corbinelli, B. Previtali, A.G. Demir, Comprehensive benchmarking of laser welding technologies including novel beam shapes and wavelengths for e-drive copper hairpins, Opt Laser Technol 169 (2024). https://doi.org/10.1016/j.optlastec.2023.109964.

[6] F. Galbusera, L. Caprio, B. Previtali, A.G. Demir, Analytical modeling and characterization of ring beam profiles for high-power lasers used in industrial manufacturing, J Manuf Process 117 (2024) 387–404. https://doi.org/10.1016/j.jmapro.2024.02.069.

[7] L. Wang, X. Gao, F. Kong, Keyhole dynamic status and spatter behavior during welding of stainless steel with adjustable-ring mode laser beam, J Manuf Process 74 (2022) 201–219. https://doi.org/10.1016/j.jmapro.2021.12.011.

[8] M. Mohammadpour, L. Wang, F. Kong, R. Kovacevic, Adjustable ring mode and single beam fiber lasers: A performance comparison, Manuf Lett 25 (2020) 50–55. https://doi.org/10.1016/j.mfglet.2020.07.003.

[9] S. Jabar, A. Baghbani Barenji, P. Franciosa, H.R. Kotadia, D. Ceglarek, Effects of the adjustable ring-mode laser on intermetallic formation and mechanical properties of steel to aluminium laser welded lap joints, Mater Des 227 (2023). https://doi.org/10.1016/j.matdes.2023.111774.

[10] W.M. Steen, J. Mazumder, Laser material processing, Springer London, 2010. https://doi.org/10.1007/978-1-84996-062-5.

[11] M. Rasch, C. Roider, S. Kohl, J. Strauß, N. Maurer, K.Y. Nagulin, M. Schmidt, Shaped laser beam profiles for heat conduction welding of aluminium-copper alloys, Opt Lasers Eng 115 (2019) 179–189. https://doi.org/10.1016/j.optlaseng.2018.11.025.

[12] R. Fabbro, Melt pool and keyhole behaviour analysis for deep penetration laser welding, J. Phys. D: Appl. Phys (2010). https://doi.org/10.1088/0022-3727/43/44/445501.

[13] Z. Wang, M. Jiang, X. Chen, Y. Du, Z. Lei, S. Zhao, Y. Chen, Mitigating spatters in keyhole-mode laser welding by superimposing additional ring-shaped beam, Opt Laser Technol 168 (2024). https://doi.org/10.1016/j.optlastec.2023.109869.